



Rapid Communication

Menthoxotriazine modified poly (ethylene terephthalate) for constructing anti-adhesion surface

Pengfei Zhang¹, Mei Yang¹, Jiyu Li, Zixu Xie, Guofeng Li, Xing Wang*

Beijing Laboratory of Biomedical Materials, College of Life Science and Technology, Beijing University of Chemical Technology, Beijing 100029, PR China



ARTICLE INFO

Keywords:

Antimicrobial adhesion
Menthol
Menthoxotriazine
PET
Stereochemistry strategy

ABSTRACT

Polyethylene terephthalate (PET) is powerless against microbial contamination, which poses a threat to human health. Thus, endowing PET with anti-adhesion surface, but without releasing germicide, is currently still a challenge. To address this issue, a menthoxotriazine modified PET (PMET) was developed based on stereochemistry strategy, through inserting the menthoxotriazine block into the chain of PET. Antibacterial adhesion test and antifungal landing test were employed to verify the anti-adhesion performances of PMET. Compared with PET, PMET possessed better anti-adhesion capacity, achieving 90.2% and 87.7% resistance to *Escherichia coli* (Gram-negative) and *Staphylococcus aureus* (Gram-positive), and a clear surface without any spores of *Aspergillus niger* (fungi). In-depth analysis revealed that the exposure of menthoxy group on PMET skeleton is crucial for antimicrobial adhesion, otherwise the wind of menthoxy group in the control polymer shows less effect. Furthermore, PMET has no cytotoxicity, thus showing excellent potential for enhancing the anti-adhesive surface of PET.

1. Introduction

Polyethylene terephthalate (PET) is one of the most commonly-used polyester materials. However, the raw PET has less antimicrobial properties. The PET-based products often provide a “hotbed” for microbial adhesion and growth [1]. A series of problems caused by microbial contamination of PET products, such as medical infection and food safety, make the urgent demand of antimicrobial PET. With the increasing health consciousness of human beings, especially in the case of COVID-19 pandemic, many efforts have been made to develop the antimicrobial PET.

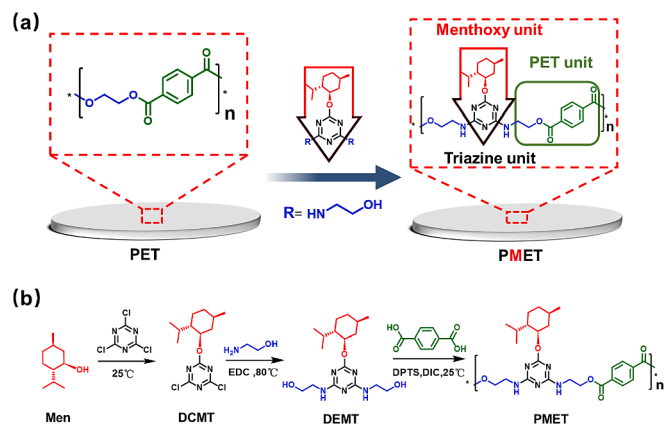
At present, to endow PET a strong killing effect on bacteria or fungi, most of the antimicrobial modification strategies of PET focus on introducing antimicrobial active substances, such as quaternary ammonium salts (QAS) [2], metal nanoparticles [3], and *N*-halamine [4], into PET by blending [5], coating [6], or grafting methods [7]. However, the microbial killing mechanism is generally worrying for their cytotoxicity and drug resistance [8–11]. It has also been reported that the antimicrobial ability may decline because of the dead microorganisms attached to the material surface [12]. Therefore, it is much-needed to develop new strategies to produce antimicrobial PET.

In recent years, a series of borneol-based materials have shown broad spectrum antimicrobial adhesion capacity based on stereochemistry strategy. Those excellent antimicrobial adhesion properties are attributed to the unique stereochemical structure of borneol molecules. The chiral structure prevents the initial adhesion of microorganisms on the material surface through the recognition of microorganisms [13]. Cellulose [14], chitosan [15], nanoparticles [16] and textiles [17–19] grafted by borneol/menthol or polymer coating [20–27] present good adhesion resistance to bacteria or fungi. Recently, triazine, a six membered ring molecule with three active chlorine atoms which easily reacts with —OH, —NH and —SH to form triazine derivatives, is employed as a suitable insertion block with functional group for polymer synthesis [28]. Therefore, introducing menthoxotriazine into PET as an antimicrobial structural unit offers an opportunity to design antimicrobial PET.

Herein, a menthoxotriazine-contained PET (PMET) is reported. As shown in Scheme 1a, menthoxotriazine group was inserted into the main chain of PET by polycondensation of terephthalic acid (TA) with 2,4-diethanolamine-6-menthoxy-1,3,5-triazine (DEMT) (Scheme 1b for the synthesis details). The anti-adhesion of PMET against *Escherichia coli* (*E. coli*, Gram-negative), *Staphylococcus aureus* (*S. aureus*, Gram-positive)

* Corresponding author.

E-mail address: wangxing@mail.buct.edu.cn (X. Wang).¹ P. Z. and M. Y. contribute equally to this work.



Scheme 1. The synthesis processes of PMET. (a) Schematic diagram of PET modification strategy. (b) The synthesis steps of PMET.

and *Aspergillus niger* (*A. niger*, fungi) were investigated with antibacterial spreading test and the antifungal landing test, respectively. In addition, the anti-bacterial adhesion performance of PMET was quantitatively evaluated by classical plate counting method and optical density test. Furthermore, the effect of menthoxy and the influence of the main chain of the polyester on the stereochemical anti-adhesion were explored.

2. Experiment

2.1. Materials

PET was purchased from Guangdong Sumao Chemical Factory (Guangdong, China). L-menthol, 2,4,6-trimethylpyridine, terephthalic acid (TA), malt extract agar, tryptone soy agar (TSA), trypticase soy broth (TSB), ethanolamine, diisopropylcarbodiimide (DIC) and 1,3,5-triazine were purchased from J&K Scientific. 4-(Dimethylamino)pyridinium-4-toluenesulfonate (DPTS) was prepared according to literature methods [29]. All the solvents were purchased from Tianjin Da Mao Chemical Reagent Factory. *Escherichia coli* (*E. coli*, ATCC 25922), *Staphylococcus aureus* (*S. aureus*, ATCC 25923) and *Aspergillus niger* (*A. niger*, CICC 41254) were obtained from the China Center of Industrial Culture Collection. Mouse fibroblast cells (L929) were obtained from Cell Resource Center, IBMS, CAMS/PUMC, Beijing, China.

2.2. Synthesis of 2,4-dichloro-6-menthoxy-1,3,5-triazine (DCMT)

In a typical procedure, L-menthol (9.36 g, 0.06 mmol), 1,3,5-triazine (5.53 g, 0.03 mmol) and 2,4,6-trimethylpyridin (4 mL, 0.04 mmol) was dissolved in 20 mL dichloromethane (DCM) and reacted at 0 °C for 12 h. The mixture was washed three times with deionized water. The organic layer was filtered and concentrated under vacuum. Further purification by silica gel column chromatography (200–300 mesh, Sinopharm Chemical Reagent Co., Ltd., China, the eluents were petroleum ether/DCM = 5:1) with 80% yield.

2.3. Synthesis of 2,4-diethanolamine-6-menthoxy-1,3,5-triazine (DEMT)

The DCMT (1.82 g, 0.006 mmol) and ethanolamine (3.66 g, 0.06 mmol) were dissolved in 20 mL of 1,2-dichloroethane. The reaction was refluxed for 8 h at 80 °C. The mixture was washed three times with deionized water. The organic layer was filtered and concentrated under vacuum, affording the desired product as a white powder at 80% yield.

2.4. Synthesis of Poly (menthoxytriazine-ethylene terephthalate) (PMET)

The PMET was synthesized by room temperature polymerization as previously reported [30]. DEMT (0.50 g, 2 mmol), TA (0.33 g, 2 mmol),

DPTS (0.03 g, 0.5 mmol) and DIC (1.5 mL, 1.5 mmol) were dissolved in 1 mL DCM and continue to react for 12 h at 25 °C under nitrogen atmosphere. The crude product was dissolved in DCM and precipitated 3 times in methanol. The final product was obtained after dryness with 75% yield.

2.5. Characterization

Fourier transform infrared (FTIR) spectra were recorded on a Nicolet Avatar-360 using KBr pellets. ¹H NMR spectra were recorded on Bruker AV-500 spectrometer using DMSO as a solvent and tetramethylsilane (TMS) as the internal reference. Gel permeation chromatography (GPC) measurements were carried out with an Agilent instrument (Model 1100). Contact angles were measured with a CA-XP150 contact angle goniometer at room atmosphere to detect the hydrophilicity of the polymer.

2.6. Bacterial anti-adhesion assays

The antibacterial spreading test was carried out by employing two typical bacteria: *E. coli* (Gram-negative) and *S. aureus* (Gram-positive) to investigate anti-adhesion properties of the PMET. PMET was pressed into 13 mm diameter sized pellet (thickness = 0.75 mm), and PET pellet was used as the control group. The sterilized pellets were affixed onto the beef extract peptone medium. Then small circular sterile media was fixed on the pellet to form a sandwich structure. 2 μL bacterial suspension (10⁶ CFU mL⁻¹) prepared in advance (the detailed method can be referred to literature [26]) was added on each of the small circular media and cultured at 37 °C. The results were recorded at intervals by a camera.

Classical plate count assays and optical density (OD) test were used to quantitatively assess the anti-bacterial adhesion properties of PMET [31]. Sterilized material were first immersed in 1 mL of *E. coli* or *S. aureus* suspension (10⁶ CFU mL⁻¹) for 24 h. Then, the material was gently rinsed three times with sterile water to remove the floating bacteria from the surface. The material was submerged in 2 mL of sterile saline and sonicated to disperse the bacteria strongly adhering to the surface of the material. Then 0.1 mL of the dispersion was applied to TSA medium and incubated at 37 °C for 24 h. For OD test, after a gentle rinsing step, material was placed in 50 mL of sterile liquid LB (Luria-Bertani) medium and incubated at 37 °C with shaking (200 rpm). The growth curves of *E. coli* and *S. aureus* were obtained by monitoring the change in OD at 600 nm at different intervals (3, 6, 9, 12, 15, 18, 21, 24 h).

2.7. Fungal anti-adhesion tests

The antifungal behavior of PMET was studied by the landing test using *A. niger* as a model fungus. 10 μL *A. niger* suspension (10⁶ CFU mL⁻¹) prepared in advance (the detailed preparation can be referred to literature [20]) was added on the center of the plate. Sterilized PMET pellet (diameter = 13 mm, thickness = 0.75 mm) were fixed on plate about 15 mm away from the center. The plate was put into the incubator at 30 °C, and the experimental phenomena were recorded by taking photos at intervals. PET was used as a control group to repeat the above experiment.

2.8. MTT assays

Cell toxicity of PMET was evaluated by MTT assay with L929 mouse fibroblasts (purchased from Cell Resource Center, IBMS, CAMS/PUMC, Beijing, China). Briefly, 0.2 g sterilized the material was immersed in 2 mL 1640 medium for 24 h. The extract was used as complete cell medium after the addition of 10% FBS, 100 units mL⁻¹ penicillin, and 100 μg mL⁻¹ streptomycin. L929 mouse fibroblasts cells were cultured in the conditioned medium at 37 °C in a humidified environment of 95% air

and 5% CO₂. After 48 h of incubation, cell viability was determined by MTT colorimetric assays. The relative growth rate (RGR) of the cells was calculated by $RGR (\%) = \text{Abs}_{490 \text{ sample}} / \text{Abs}_{490 \text{ control}} \times 100$, where $\text{Abs}_{490 \text{ sample}}$ and $\text{Abs}_{490 \text{ control}}$ are the absorbance of the samples and the reference at 490 nm, respectively.

3. Results and discussion

3.1. Synthesis and characterization of PMET

The FTIR spectra of the PMET, compared with those of Men, DCMT and DEMA are shown in Fig. 1a. In the FTIR spectra of the DCMT (Fig. 1a, red), the absorption band of O–H stretching of the hydroxyl groups at 3300 cm⁻¹ completely disappeared. Meanwhile, the absorption peaks appeared at 1500 cm⁻¹ due to the presence of the absorption band characteristic of stretching vibrations of the TCT (–C=N–) group. Compared with DCMT, a new absorption band corresponding to the O–H and N–H stretching absorption of the DEMA (Fig. 1a, blue) could be observed at 3350 cm⁻¹. In terms of PMET (Fig. 1a, green), characteristic absorption bands for C=C aromatic vibration appeared at around 1260 and 810 cm⁻¹. In addition, the presence of the ester was shown by the C=O stretching peaks of the carbonyl group at the strong absorption at 1720 cm⁻¹. Moreover, the absorption peaks at 1020 cm⁻¹ were assigned to the C–O stretching of the ether groups.

The ¹H NMR spectra of the PMET, compared with those of Men, DCMT and DEMA, were recorded in order to confirm the structure of the polymer (Fig. 1b). In the ¹H NMR spectra of the DCMT (Fig. 1b, red), the distinct signals at 0.70–2.08 ppm due to the aromatic protons of Men. And the resonance signal of hydroxyl group at 4.2 ppm disappeared. In terms of the DEMA (Fig. 1b, blue), the protons of imino group appeared at 7.02 ppm and 6.90 ppm. And the signals observed at 4.83 ppm, 3.46 ppm and 3.33 ppm were protons of the hydroxyl group and methylene group, respectively. In the ¹H NMR spectrum of PMET (Fig. 1b, green), the proton of hydroxyl group at 9.41 ppm disappeared. The resonance of aromatic protons appeared at 7.98 ppm.

The results of molecular weight and polydispersity index (PDI) of PMET were summarized in Table S1. The molecular weights of the PMET were above 10⁴ g mol⁻¹ and PDI was 1.02, indicating the high-molecular-weight and the narrow distribution of relative molecular mass of polymer. These evidences proved that the PMET was synthesized successfully.

3.2. Bacterial anti-adhesion assays

Antibacterial spreading test (Fig. 2a) was used to evaluate the anti-bacterial adhesion ability of the PMET against *E. coli* and *S. aureus*. It

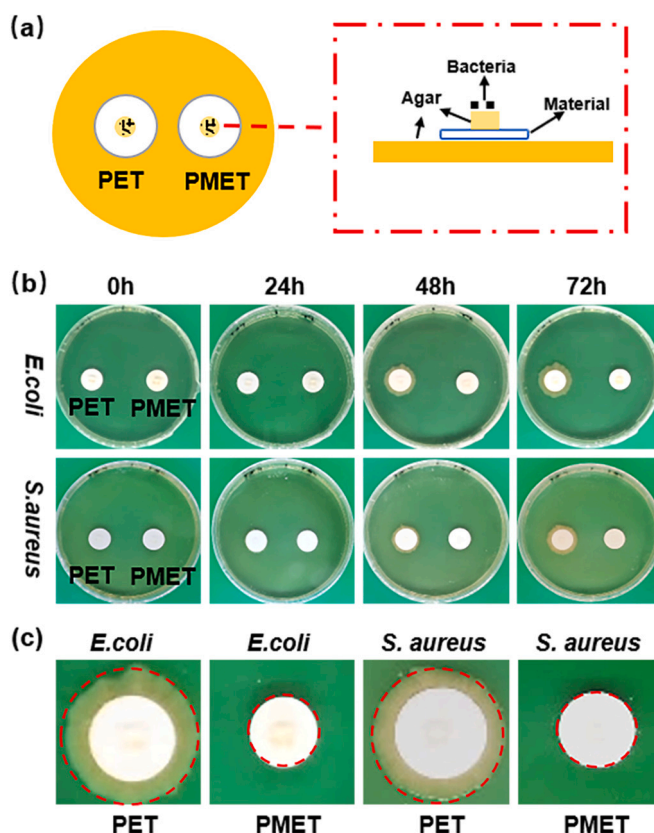


Fig. 2. Antibacterial spreading test of PMET. (a) Schematic illustration of antibacterial spreading test. (b) Digital photos of the antibacterial spreading test of PET and PMET. (c) Enlarged images of the antibacterial spreading test of PET and PMET at 72 h.

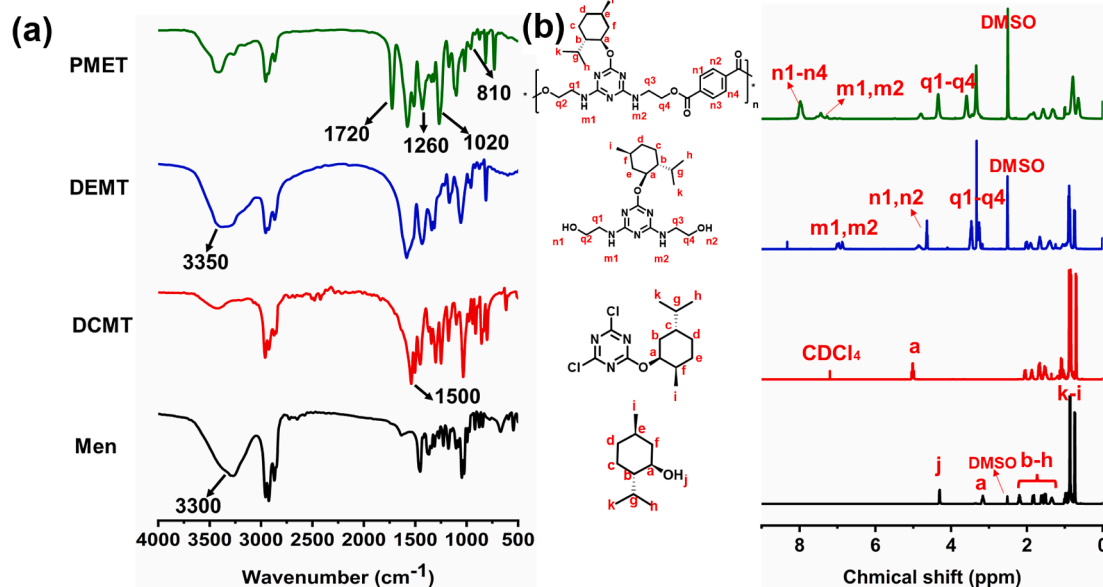


Fig. 1. Characterization of Men, DCMT, DEMA and PMET. (a) FTIR spectra. (b) ¹H NMR spectra. (For interpretation of the references to color in this figure, the reader is referred to the web version of this article.)

could be observed that no *E. coli* on the PMET group was observed on the medium at 24 h, but a little *E. coli* could be seen at PET group (Fig. 2b). After 48 h. *E. coli* grew beyond the PET and obvious bacterial ring appeared on the culture medium, indicating that PET did not inhibit the growth of *E. coli*. In contrast, *E. coli* had not broken the limit of PMET until 72 h (Fig. 2c). Thus, PMET showed good capacity for inhibiting the expansion of *E. coli*. Moreover, Gram-positive *S. aureus* was employed to challenge the PMET (Fig. 2b) in order to further evaluate its broad-antiadhesion properties. The PET was broken after 24 h, and *S. aureus* did not spread out of PMET until 72 h, demonstrating that the PMET could effectively inhibit the growth of *S. aureus*.

The anti-bacterial adhesion properties of PMET were also studied quantitatively using the classical plate counting method. As shown in Fig. 3a, the number of *E. coli* colonies on PMET was 58, while the number of *E. coli* colonies on PET was 589 units, which was about 10 times higher than that of PMET. The number of *S. aureus* colonies on PET (685 units) was about 8 times higher than that of colonies on PMET (84 units). This indicated that PMET had better resistance to bacterial (*E. coli* and *S. aureus*) adhesion compared to PET. In addition, the antibacterial adhesion rate of PMET against *E. coli* (90.2%) was slightly higher than that against *S. aureus* (87.7%). Optical density (OD) test was used to verify the above findings. As shown in Fig. 3b, after 6 h of incubation, the *E. coli* in the PET group started to enter the logarithmic growth phase, while the PMET group was still in the lag phase. After 9 h of incubation, the OD values of the two experimental groups showed a significant difference in the concentration of the bacterial solution. In addition, it could be visually observed from the inset that the liquid medium of the PET group had become visibly turbid, while in contrast, that of the PMET group remained clear. For *S. aureus*, it was observed that *S. aureus*, after 9 h of incubation, started to enter the logarithmic phase of bacterial growth. Unlike *E. coli*, the greatest difference in bacterial concentration between the PET and PMET groups was observed after 12 h. Also, it was possible to find that the PET group showed an intuitive turbidity while the PMET group remained almost transparent. Thus, PMET had good capacity for inhibiting the expansion of gram-positive and gram-negative bacteria.

3.3. Fungal anti-adhesion tests

The antifungal landing test (Fig. 4a) was used to evaluate the antifungal (*A. niger*) adhesion ability of PMET. As shown in Fig. 4b, with the fungi grew and spread, it began to contact the edge of PET and PMET at 2 d. There was a significant difference in the growth of *A. niger* between the two materials at 4 d. Spores began to cover the surface of PET, indicating that the PET had no inhibitory effect on the growth of *A. niger*,

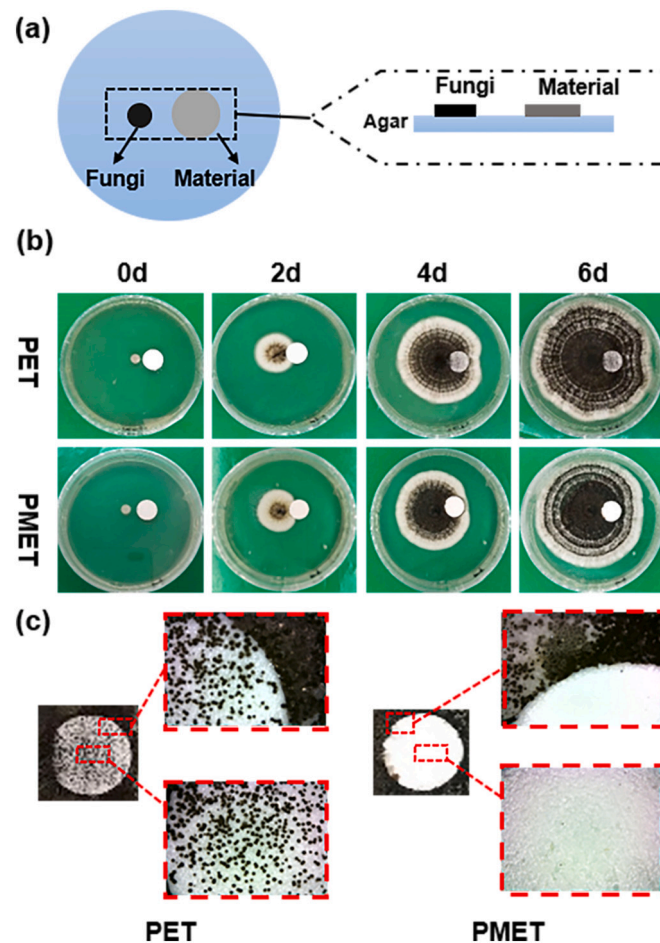


Fig. 4. The antifungal anti-adhesion test of PMET. (a) Schematic illustration of antifungal landing test. (b) Digital photos of the anti-adhesion effects of PMET and PET. (c) Enlarged images of the anti-adhesion effects of PMET and PET for 6 d.

whereas no spore was observed on the PMET. PET was almost covered by *A. niger* after 6 d. However, PMET still remained clean and blocked the growth of *A. niger* (Fig. 4c). It proved that PMET exhibit antifungal action against *A. niger*.

3.4. Mechanism of microbial anti-adhesion

The PMET was prepared by inserting menthoxy-triazine block into the main chain of PET. This polymer has a good antimicrobial adhesion capability, due to the existence of menthoxy group with stereochemical structure. In order to prove this hypothesis, PMSA was prepared as a control group (Scheme 2a). The anti-adhesive effect of PMSA on fungi and bacteria was tested separately. Antifungal landing test showed that the surface of PET was almost completely covered with fungus after 6 d (Fig. 4c). And a little *A. niger* adhesion on the surface of the PMSA. On the contrary, the PMET surface was very clean, without any *A. niger* adhered on its surface (Scheme 2b). It demonstrated that the order of the three materials in terms of anti-fungal adhesion ability was PMET > PMSA > PET. In addition, the performance of PMSA against the spread of *E. coli* was also studied (Fig. S8). *E. coli* broke through the restriction of PMSA at 48 h. In contrast, *E. coli* on PMET broke the material restriction at 72 h. Compared to PMSA and PMET, PET was breached by *E. coli* at 24 h (Fig. 2b). It indicated that PMSA was less resistant to bacterial spreading than PMET, but more resistant than PET. Due to the introduction of menthoxy groups, both PMSA and PMET exhibit stronger anti-microbial adhesion effects than PET. And the reason for the

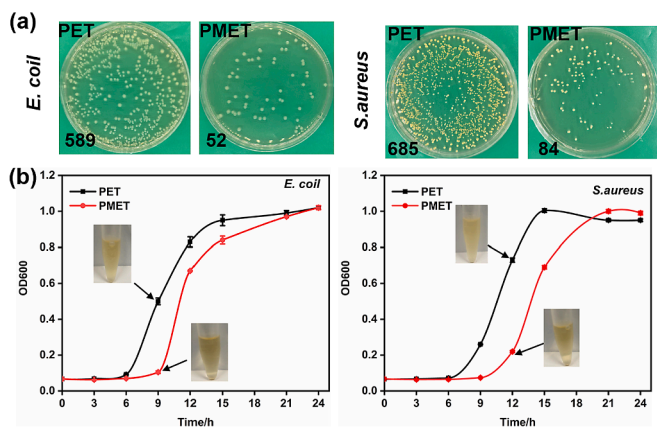
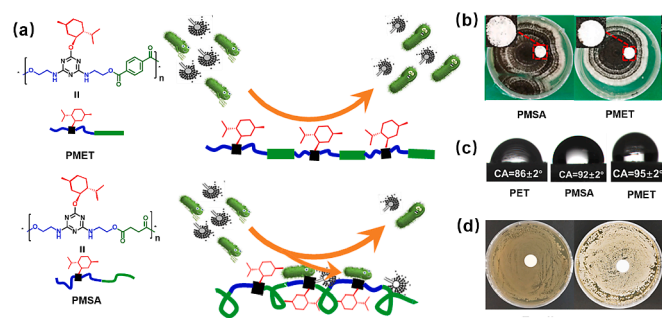


Fig. 3. Quantitative anti-bacterial adhesion test of PMET. (a) Plate count experiments of PET and PMET against *E. coli* and *S. aureus*. (b) Optical density 600 test results to evaluate the antibacterial property of PET and PMET against *E. coli* and *S. aureus*.



Scheme 2. Schematic representation of microbially antiadhesive effect. (a) Anti-adhesion mechanism of PMET and PMSA. (b) Antifungal landing test of PMET and PMSA. (c) Contact angle of PET, PMET and PMSA. (d) The inhibition zone test of PMET against *E. coli* and *S. aureus*.

different anti-adhesive ability of PMSA and PMET may be the different main chain structures of the two materials. The menthoxy unit on the main chain was wrapped by the flexible chain of PMSA, which results in less exposure of the menthoxy moiety. On the contrary, PMET has the rigid benzene group, so it has no obvious wrapping effect on the menthoxy group, resulting in most of the menthoxy being exposed in the surface of polymer. It suggests that the menthoxy structure must be exposed to sufficient amount on the material surface for playing the role of antibacterial adhesion. Water contact angle experiments were used to prove this speculation. The CA of PMET was same than that of PMSA but greater than that of PET, indicating the wettability of PMET was not the main factor affecting microbial adhesion (Scheme 2c). As shown in Scheme 2d, there are no clear zones around the disks for *E. coli* and *S. aureus*, which imply PMET didn't release antibacterial agents to achieve antimicrobial effect.

3.5. MTT assay

Good biocompatibility is important for antimicrobial materials, especially in practical applications in medicine. Cell toxicity is key index to evaluate the biocompatibility of antimicrobial materials. Therefore, MTT assay was used to evaluate the cytotoxicity of PMET. As shown in Fig. 5, the relative growth rate of cells in contact with PET and PMET materials were $93.20 \pm 9.60\%$ and $89.03 \pm 8.57\%$. According to the standard toxicity rating in the Pharmacopoeia of United States (USP, Table S3), the cell toxicity of PMET was in grade 1 (Table. S2), indicating PMET were no toxicity.

4. Conclusion

In summary, the PMET, an antimicrobial adhesive PET modified by menthoxytriazine, was prepared via a typical DIC-mediated coupling of DEMA with TA. The antibacterial spreading test demonstrated that the PMET had good antibacterial ability. The classical plate count method

Appendix A. Supplementaru data

References

- [1] M. Ersan, H. Dogan, Development of new adsorbents via microwave treatment magnetic PET synthesis from waste PET and investigation of TC removal, *Colloid Interface Sci. Commun.* 42 (2021), 100416, <https://doi.org/10.1016/j.colcom.2021.100416>.
- [2] S. Zhang, R. Li, D. Huang, X. Ren, T.S. Huang, Antibacterial modification of PET with quaternary ammonium salt and silver particles via electron-beam irradiation, *Mater. Sci. Eng. C* 85 (2018) 123–129, <https://doi.org/10.1016/j.msec.2017.12.010>.

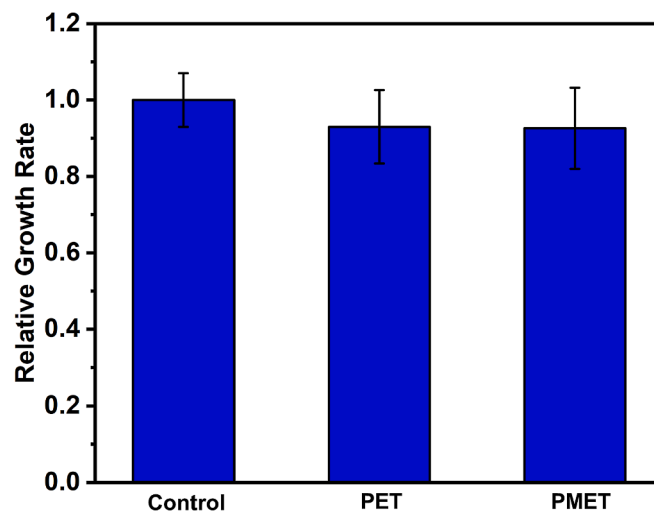


Fig. 5. MTT results of the RGR in L929 cells after 48 h of incubation with the PET and PMET conditioned medium.

and optical density test illustrated the good anti-adhesion performance of PMET by further quantitative assessment, with anti-adhesion rates of 90.2% and 87.7% against *E. coli* and *S. aureus*, respectively. In addition, the antifungal landing test showed that the PMET had good ability to inhibit the adhesion and proliferation of fungi. PMET was also a non-toxic material. Deeply insight revealed that the exposure of enough menthoxy group ensured the antimicrobial adhesion. PMET not only provides a promising candidate for antimicrobial polyester, but also demonstrates the cardinal principle of the surface stereochemistry for anti-adhesion of microorganism.

Credit author statement

Wang developed the research scheme and the draft. P Zhang and M Yang did the experiments. P Zhang wrote the manuscript. J Li tested the NMR and GPC. G Li and Z Xie took part in interpretation of data. All authors read and approved the final manuscript.

Declaration of Competing Interest

The authors declare that they have no known competing financial interests or personal relationships that could have appeared to influence the work reported in this paper.

Acknowledgments

The authors thank the National Natural Science Foundation of China (21574008) and the Fundamental Research Funds for the Central Universities of China (BHYC1705B) for their financial support.

- [3] S. Tavakoli, S. Nemati, M. Kharaziha, S. Akbari Alavijeh, Embedding CuO nanoparticles in PDMS-SiO₂ coating to improve antibacterial characteristic and corrosion resistance, *Colloid Interface Sci. Commun.* 28 (2019) 20–28, <https://doi.org/10.1016/j.colcom.2018.11.002>.
- [4] D. Chai, W. Liu, X. Hao, H. Wang, H. Wang, Y. Hao, Y. Gao, H. Qu, L. Wang, A. Dong, G. Gao, Mussel-inspired synthesis of magnetic N-halamine nanoparticles for antibacterial recycling, *Colloid Interface Sci. Commun.* 39 (2020), 100320, <https://doi.org/10.1016/j.colcom.2020.100320>.
- [5] Y. Zhao, B. Zhao, B. Wei, Y. Wei, J. Yao, H. Zhang, X. Chen, Z. Shao, Enhanced compatibility between poly(lactic acid) and poly (butylene adipate-co-

- terephthalate) by incorporation of N-halamine epoxy precursor, *Int. J. Biol. Macromol.* 165 (2020) 460–471, <https://doi.org/10.1016/j.ijbiomac.2020.09.142>.
- [6] H. Li, D. Huang, K. Ren, J. Ji, Inorganic-polymer composite coatings for biomedical devices, *Smart Mater. Med.* 2 (2021) 1–14, <https://doi.org/10.1016/j.smaim.2020.10.002>.
- [7] H. Salmi Mani, G. Terreros, N. Barroca Aubry, C. Aymes Chodur, C. Regeard, P. Roger, Poly(ethylene terephthalate) films modified by UV-induced surface graft polymerization of vanillin derived monomer for antibacterial activity, *Eur. Polym. J.* 103 (2018) 51–58, <https://doi.org/10.1016/j.eurpolymj.2018.03.038>.
- [8] X. Ding, S. Duan, X. Ding, R. Liu, F. J., Xu, versatile antibacterial materials: an emerging arsenal for combatting bacterial pathogens, *Adv. Funct. Mater.* 28 (2018) 1802140, <https://doi.org/10.1002/adfm.201802140>.
- [9] M.P. Ortega, L.M. López Marín, B. Millán Chiu, P. Manzano Gayosso, L.S. Acosta Torres, R. García Contreras, R. Manisekaran, Polymer mediated synthesis of cationic silver nanoparticles as an effective anti-fungal and anti-biofilm agent against *Candida* species, *Colloid Interface Sci. Commun.* 43 (2021), 100449, <https://doi.org/10.1016/j.colcom.2021.100449>.
- [10] T. Wei, Q. Yu, H. Chen, Responsive and synergistic antibacterial coatings: fighting against bacteria in a smart and effective way, *Adv. Healthc. Mater.* 8 (2019) 1801381, <https://doi.org/10.1002/adhm.201801381>.
- [11] C. Zhang, Y. Li, C. Ma, Q. Zhang, Recent progress of organic-inorganic hybrid perovskites in RRAM, artificial synapse, and logic operation, *Small Sci.* (2021) 2100086, <https://doi.org/10.1002/smssc.202100086>.
- [12] S. Kokilavani, A. Syed, H.A.A.L. Shwaiman, M.M. Alkhulaifi, F.N. Almajdhi, A. M. Elgorban, S.S. Khan, Preparation of plasmonic CoS/Ag₂WO₄ nanocomposites: efficient visible light driven photocatalysts and enhanced anti-microbial activity, *Colloid Interface Sci. Commun.* 42 (2021), 100415, <https://doi.org/10.1016/j.colcom.2021.100415>.
- [13] G. Li, H. Zhao, J. Hong, K. Quan, Q. Yuan, X. Wang, Antifungal graphene oxide-borneol composite, *Colloids Surf. B: Biointerfaces* 160 (2017) 220–227, <https://doi.org/10.1016/j.colsurfb.2017.09.023>.
- [14] B. Shi, D. Luan, S. Wang, L. Zhao, L. Tao, Q. Yuan, X. Wang, Borneol-grafted cellulose for antifungal adhesion and fungal growth inhibition, *RSC Adv.* 5 (2015) 51947–51952, <https://doi.org/10.1039/c5ra07894f>.
- [15] Y. Xin, H. Zhao, J. Xu, Z. Xie, G. Li, Z. Gan, X. Wang, Borneol-modified chitosan: antimicrobial adhesion properties and application in skin flora protection, *Carbohydr. Polym.* 228 (2020), 115378, <https://doi.org/10.1016/j.carbpol.2019.115378>.
- [16] X. Chen, Q. Nie, Y. Shao, Z. Wang, Z. Cai, TiO₂ nanoparticles functionalized borneol-based polymer films with enhanced photocatalytic and antibacterial performances, *Environ. Technol. Innov.* 21 (2021), 101304, <https://doi.org/10.1016/j.eti.2020.101304>.
- [17] J. Xu, H. Zhao, Z. Xie, S. Ruppel, X. Zhou, S. Chen, J.F. Liang, X. Wang, Stereochemical strategy advances microbially antiadhesive cotton textile in safeguarding skin flora, *Adv. Healthc. Mater.* 8 (2019) 1–10, <https://doi.org/10.1002/adhm.201900232>.
- [18] J. Xu, Z. Xie, F. Du, X. Wang, One-step anti-superbug finishing of cotton textiles with dopamine-menthol, *J. Mater. Sci. Technol.* 69 (2021) 79–88, <https://doi.org/10.1016/j.jmst.2020.08.007>.
- [19] L. Yang, C. Zhan, X. Huang, L. Hong, L. Fang, W. Wang, J. Su, Durable antibacterial cotton fabrics based on natural borneol-derived anti-MRSA agents, *Adv. Healthc. Mater.* 9 (2020) 1–8, <https://doi.org/10.1002/adhm.202000186>.
- [20] C. Chen, Z. Xie, P. Zhang, Y. Liu, X. Wang, Cooperative enhancement of fungal repelling performance by surface photografting of stereochemical bi-molecules, *Colloids Interface Sci. Commun.* 40 (2021), 100336, <https://doi.org/10.1016/j.colcom.2020.100336>.
- [21] Q. Cheng, A.B. Asha, Y. Liu, Y.Y. Peng, D. Diaz Dussan, Z. Shi, Z. Cui, R. Narain, Antifouling and antibacterial polymer-coated surfaces based on the combined effect of zwitterions and the natural borneol, *ACS Appl. Mater. Interfaces* 13 (2021) 9006–9014, <https://doi.org/10.1021/acsami.0c22658>.
- [22] X. Chen, Y. Chen, S. Lv, L. Zhang, R. Ye, C. Ge, D. Huang, S. Zhang, Z. Cai, New type of borneol-based fluorine-free superhydrophobic antibacterial polymeric coating, *Des. Monomers Polym.* 24 (2021) 147–157, <https://doi.org/10.1080/15685551.2021.1924959>.
- [23] F. Song, L. Zhang, R. Chen, Q. Liu, J. Liu, J. Yu, P. Liu, J. Duan, J. Wang, Bioinspired durable antibacterial and antifouling coatings based on borneol fluorinated polymers: demonstrating direct evidence of antiadhesion, *ACS Appl. Mater. Interfaces* 13 (2021) 33417–33426, <https://doi.org/10.1021/acsami.1c06030>.
- [24] C. Zhang, J. Guo, X. Zou, S. Guo, Y. Guo, R. Shi, F. Yan, Acridine-based covalent organic framework photosensitizer with broad-spectrum light absorption for antibacterial photocatalytic therapy, *Adv. Healthc. Mater.* 2100775, <https://doi.org/10.1002/adhm.202100775>.
- [25] Z. Lu, Y. Wu, Z. Cong, Y. Qian, X. Wu, N. Shao, Z. Qiao, H. Zhang, Y. She, K. Chen, H. Xiang, B. Sun, Q. Yu, Y. Yuan, H. Lin, M. Zhu, R. Liu, Effective and biocompatible antibacterial surfaces via facile synthesis and surface modification of peptide polymers, *Bioact. Mater.* 6 (2021) 4531–4541, <https://doi.org/10.1016/j.bioactmat.2021.05.008>.
- [26] X. Sun, Z. Qian, L. Luo, Q. Yuan, X. Guo, L. Tao, Y. Wei, X. Wang, Antibacterial adhesion of poly(methyl methacrylate) modified by borneol acrylate, *ACS Appl. Mater. Interfaces* 8 (2016) 28522–28528, <https://doi.org/10.1021/acsami.6b10498>.
- [27] L. Luo, G. Li, D. Luan, Q. Yuan, Y. Wei, X. Wang, Antibacterial adhesion of borneol-based polymer via surface chiral stereochemistry, *ACS Appl. Mater. Interfaces* 6 (2014) 19371–19377, <https://doi.org/10.1021/am505481q>.
- [28] S.H. Yoo, Y.W. Kim, K. Chung, N.K. Kim, J.S. Kim, Corrosion inhibition properties of triazine derivatives containing carboxylic acid and amine groups in 1.0 M HCl solution, *Ind. Eng. Chem. Res.* 52 (2013) 10880–10889, <https://doi.org/10.1021/ie303092j>.
- [29] E.A. Chamsaz, S. Mankoci, H.A. Barton, A. Joy, Nontoxic cationic coumarin polyester coatings prevent *Pseudomonas aeruginosa* biofilm formation, *ACS Appl. Mater. Interfaces* 9 (2017) 6704–6711, <https://doi.org/10.1021/acsami.6b12610>.
- [30] E.A. Chamsaz, S. Mankoci, H.A. Barton, A. Joy, Nontoxic cationic coumarin polyester coatings prevent *Pseudomonas aeruginosa* biofilm formation, *ACS Appl. Mater. Interfaces* 9 (2017) 6704–6711, <https://doi.org/10.1021/acsami.6b12610>.
- [31] J. Wu, C. Wang, C. Mu, W. Lin, A waterborne polyurethane coating functionalized by isobornyl with enhanced antibacterial adhesion and hydrophobic property, *Eur. Polym. J.* 108 (2018) 498–506, <https://doi.org/10.1016/j.eurpolymj.2018.09.034>.